JACS
JOURNAL OF THE AMERICAN CHEMICAL SOCIETY
pubs.acs.org/JACS
Article

Air-Stability and Carrier Type in Conductive M_3(Hexaaminobenzene)$_2$, (M = Co, Ni, Cu)

Allison C. Hinckley,[#] Jihye Park,[#] Joseph Gomes, Evan Carlson, and Zhenan Bao*

Cite This: https://dx.doi.org/10.1021/jacs.0c03500

ABSTRACT: Herein, we investigate the effects of changing the metal ions in the M-HAB system, with HAB = hexaaminobenzene ligands and M = Co, Ni, Cu. The phyiscal characteristics of this MOF family are insensitive to changes in the metal cation, which enables systematic evaluation of the effect of metal cation identity on electrical transport properties. We observe that the metal ion profoundly influences the electrical conductivity and dominant carrier type in the resulting MOF and the air-stability thereof. Cu-HAB and Co-HAB are determined to exhibit n-type conduction under both ambient and nitrogen conditions; Ni-HAB is found to be ambipolar, with its dominant carrier type dramatically affected by the environment. We examine these results through calculation of the band structure, the partial density of states, and charge transfer analysis. Unlike traditional conductive organic materials, we find that the air-stability is not well predicted by the LUMO level of these n-type MOFs but instead is additionally dependent on the occupancy and orientation of the metal ion's *d*-orbitals and the resulting interaction between the metal ion and ligand. This study provides fundamental insights for rational design of air-stable, electronically conductive MOFs.

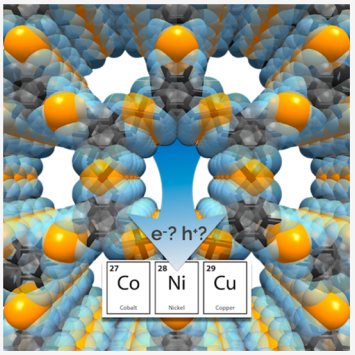

INTRODUCTION

Reports of a newly emerging subclass of electrically conductive, two-dimensional (2D) metal−organic frameworks (MOFs) have elicited great interest due to their unique combination of electronic conduction and extensive, predictable structure.[1−17] Several comprehensive reports on the recent progress of conductive MOFs and their employment have been published.[18−25] MOFs are hybrid materials composed of organic segments linked by metal atoms to form an extended porous, crystalline structure. The ability to leverage the synthetic toolboxes of both organic and inorganic chemistry to precisely tailor the structure and thus function of these materials is therefore one of their major advantages.[26] Moreover, the MOF's defined and extended lattice structure and the potentially large carrier population suggest a route to higher electrical conductivities than that achieved by fully organic systems. As yet, the record bulk MOF conductivity is an order of magnitude less than that of high performing polymeric systems, so there is still much room for improvement.[27−29] A further advantage of MOFs is that the coupling between the organic and inorganic moieties may overcome the air-instability generally associated with mobile electrons in fully organic systems.[30] N-type organic conductivities typically lag behind those of p-type organic materials due to the susceptibility of mobile electrons to trap states created through exposure to oxygen or water.[31,32] Fluorinated metallophthalocyanines are examples of air-stable n-type organic semiconductors with metals incorporated into larger organic structures.[33]

MOFs could thus fill the demand for air-stable and synthetically facile electronic materials; however, realization of their potential requires a greater understanding of how the metal ions and ligands in the MOF affect conductance. There is overall a dearth of systematic studies that characterize how the MOF components affect bulk MOF electronic properties due to the synthetic challenges of preparing a variety of candidates in a single MOF family.[34] Herein, we report on the influence of the metal ion in a two-dimensional, conductive MOF system on the electronic structure and conductance. The MOF structures employed in this work are composed of hexaaminobenzene (HAB) as the organic linker and divalent cations of copper, cobalt, and nickel as the metal nodes.

A depiction of the M-HAB (M = Co, Ni, Cu) structure is shown in Figure 1A. For this study, we chose the M-HAB system because of the synthetic capability to control its physical characteristics. It is important that the materials adopt the same crystal packing structure and comparable particle size and morphologies in order to observe the dependence of the electronic properties on the metal ion as opposed to different transport pathways or path-lengths.[35] The M-HAB system is known to adopt a square planar structure for all three metal

Received: March 30, 2020
Published: May 30, 2020

https://dx.doi.org/10.1021/jacs.0c03500
J. Am. Chem. Soc. XXXX, XXX, XXX−XXX

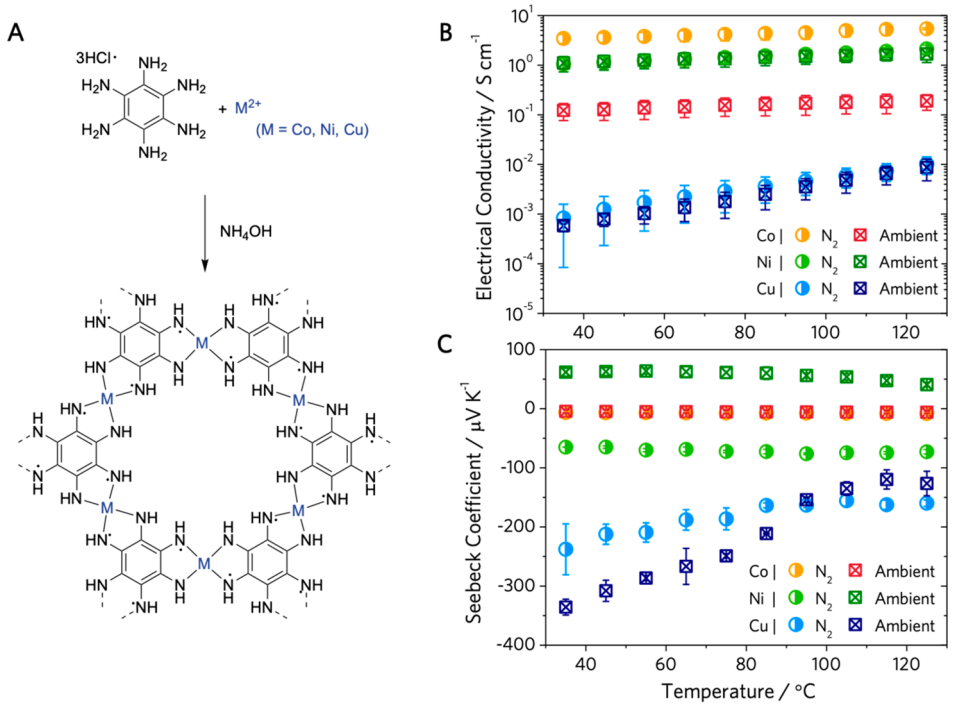

Figure 1. (A) Synthetic scheme of M-HAB, (B) electrical conductivity, and (C) Seebeck coefficient of M-HABs under nitrogen and ambient conditions from a minimum of three different batches of samples for each condition.

ions, resulting in the same MOF crystal structures, as reported previously.[14,36] Another key feature of the M-HAB MOFs is their inherent semiconductivity or conductivity without intentional doping or contributions from conductive additives, which allows for study of the particular interaction between the metal atom and organic linker.

RESULTS AND DISCUSSION

With the aim of developing air-stable and practical electronic materials, the electrical conductivity was measured on bulk, pressed-powder M-HAB pellets under both nitrogen and ambient conditions; the results are summarized in Figure 1B. The particle sizes in the powder are around 20−40 nm for all cases by controlling the synthesis conditions. The difference in absolute conductivity values of Ni-HAB and Cu-HAB reported here from those reported by Dinca et al. is possibly due to the different crystal packing structure observed for the M-HAB MOFs synthesized using the method we reported previously.[13,14] As shown, the magnitude of the bulk electrical conductivity under nitrogen and ambient conditions varies significantly with the different metal ions. Only Co-HAB exhibits significant decline in the electrical conductivity, retaining a mere 3.5% of its inert performance when measured under ambient conditions. The inert electrical conductivity for all M-HABs can be fully restored after ambient exposure by baking the samples for 1 h at 120 °C. M-HAB MOFs all exhibit thermally activated transport, as shown by their increasing conductivity with temperature as shown in Figure 1B. The thermally activated transport could be attributed to multiple factors: (1) hopping transport given the many grain boundaries (~2 nm average grain size) and traps in these bulk, pressed powder materials and (2) their semiconducting nature, as evidenced by their reported optical bandgaps of 0.74, 0.57, and 0.87 eV for Cu-HAB, Ni-HAB, and Co-HAB, respectively.[14,36] Separation of the individual contributions to the temperature-dependence of the conductivity from charge-carrier generation and transport requires knowledge of the temperature dependence of the Seebeck coefficient of these materials.

The Seebeck coefficients of the pressed MOF pellets were measured under conditions identical to those of the conductivity measurements. The Seebeck coefficient quantifies the thermoelectric potential gradient induced by a temperature gradient across a given material; for an n-type material, the Seebeck coefficient is usually negative. As shown in Figure 1C, all M-HABs exhibit n-type behavior under nitrogen conditions. The magnitude as well as sign of the Seebeck coefficient is revealing of the carrier populations present in the M-HAB system. Despite its thermally activated transport and optical bandgap, Co-HAB exhibits a Seebeck coefficient <10 μV K^{-1} in magnitude, which is typical of metallic materials. The slight drop in magnitude of the Seebeck coefficient (see Supporting Information) and simultaneous large drop in the electrical conductivity when Co-HAB is exposed to ambient conditions is a significant result, as it represents a decoupling of these traditionally coupled variables. The magnitude and sign of S for bulk Co-HAB is similar to the reported values of thin films of other high-conductivity coordination compounds, measured under a vacuum.[17,37] The Seebeck coefficient of Cu-HAB is nearly 2 orders of magnitude higher than that of Co-HAB and similar in magnitude to $Cu_3(BTC)_2$, a Cu-based 3D MOF with BTC = benzene-1,3,5-tricarboxylate, doped with TCNQ (7,7,8,8-tetracyanoquinodimethane).[38] Unlike Cu-HAB, $Cu_3(BTC)_2$ is not inherently conductive and exhibits conductivity on the order of 10^{-10} S cm^{-1} without doping. The positive Seebeck coefficient of $Cu_3(BTC)_2$ is attributed to the p-type dopant, TCNQ. With air exposure, the Seebeck coefficient of Cu-HAB increases in magnitude and retains sign, most likely indicating p-type doping in an n-type material. Ni-HAB exhibits more extensive p-type doping under ambient conditions, with a near complete carrier population inversion

https://dx.doi.org/10.1021/jacs.0c03500
J. Am. Chem. Soc. XXXX, XXX, XXX−XXX

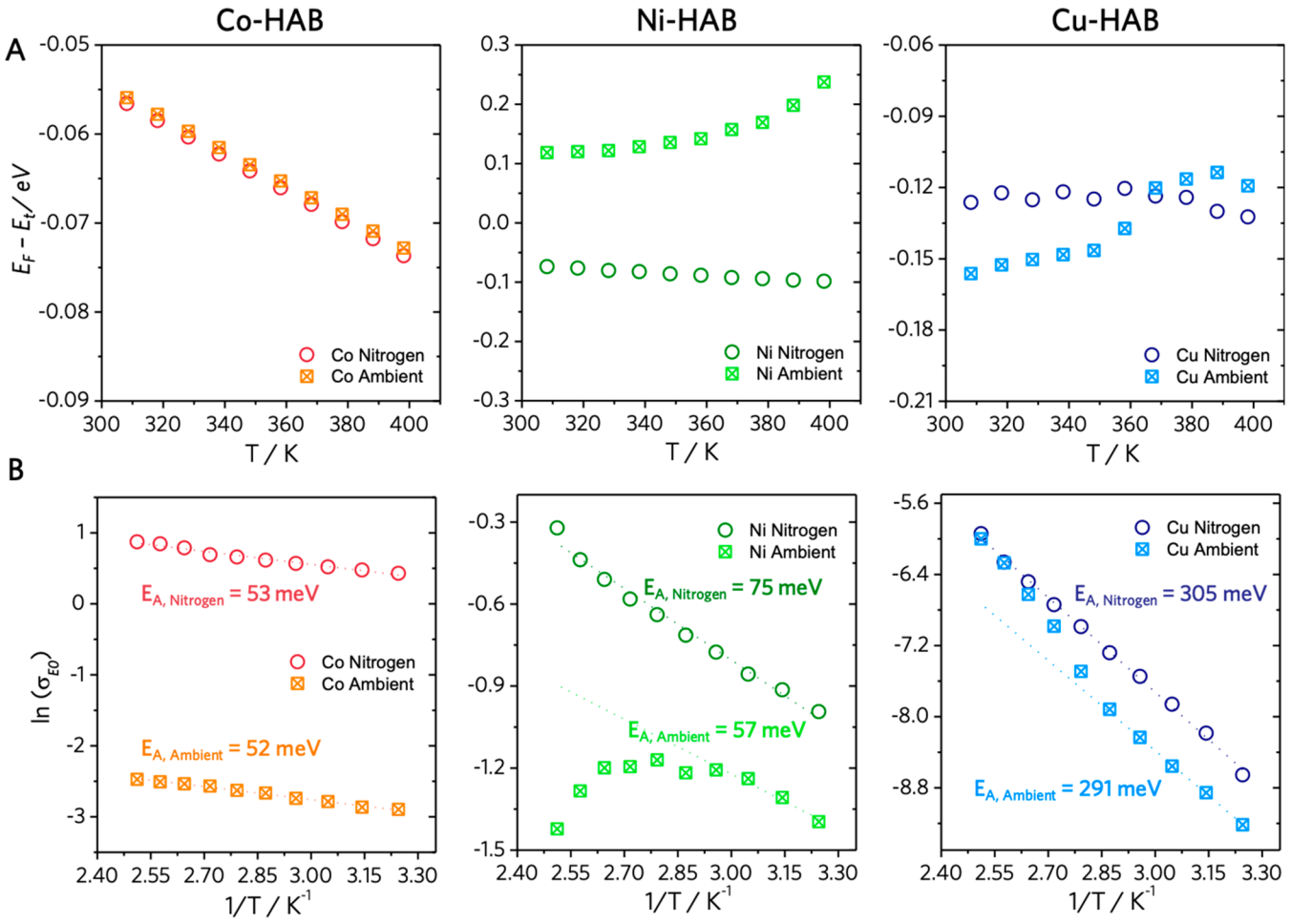

Figure 2. (A) Temperature dependence of the energy offset between the Fermi energy and transport edge energy of M-HABs under nitrogen and ambient conditions calculated with eqs S11 and S12. (B) The temperature-dependent transport coefficient $\sigma_{E_0}(T)$ calculated with eq S10. Dotted lines are the fit to a thermally activated hopping model (eq 2).

as evidenced in the change in the Seebeck coefficient from −65.1 μV K^{-1} under nitrogen conditions to +61.8 μV K^{-1} under ambient conditions at 300 K. Ni-HAB thus fits into the growing class of Ni-based ambipolar materials, such as the Ni-dithiolene derivatives that have demonstrated an ambipolar field-effect transistor performance.[39] Ni_3HITP_2 (HITP = hexaiminotriphenylene), another 2D conductive MOF, demonstrated ambipolar behavior as well, with a negative Seebeck coefficient under a vacuum and p-type performance in a FET under ambient conditions.[7,40]

To gain a greater understanding of the charge transport processes in these conductive MOFs, the temperature-dependent component of the transport function, $\sigma_{E_0}(T)$, and the reduced chemical potential, η, were calculated from the Seebeck and conductivity data using the Kang-Snyder model.[41] The specific calculations performed are discussed in greater detail in the Supporting Information. Figure 2A depicts the difference between the electron chemical potential, E_F, and the transport edge energy, E_t, determined through the relation

$$\eta = \frac{E_F - E_t}{k_B T} \quad (1)$$

As shown, all M-HABs exhibit a trend toward increasing $|E_F - E_t|$ with increasing temperature under nitrogen conditions, consistent with the generation of thermally excited carriers. Under ambient conditions, the behavior varies significantly with the metal node. For Co-HAB, E_F is shifted ∼0.7 meV toward the transport edge, consistent with minor n-type doping, but retains linear dependence on temperature. For Ni-HAB, $|E_F - E_t|$ increases exponentially with temperature under ambient conditions, which signifies decreasingly effective p-type doping and is consistent with the p-type doping occurring via physisorption of O_2 or H_2O in air. As the temperature increases, the physisorption is destabilized, and fewer n-type carriers are trapped. The Fermi level of Cu-HAB is fairly constant under nitrogen conditions, but deviation from linear behavior is evident under ambient conditions. The 30 meV shift in E_F away from the transport edge indicates that Cu-HAB is p-type doped in air at moderate temperatures (<360 K). Above 350 K, the doping is destabilized and Cu-HAB exhibits a small degree of n-type doping. After baking under nitrogen or vacuum conditions at 120 °C for all M-HABs, the performance of nitrogen-treated sample is restored, further corroborating the physisorption model.

The Kang-Snyder model allows for separation of the contributions to the electrical conductivity from thermally activated charge carrier generation and from thermally activated transport, e.g. hopping or variable-range hopping.[41] The calculated temperature-dependent transport function, $\sigma_{E_0}(T)$, was then fit to a thermally activated hopping model

https://dx.doi.org/10.1021/jacs.0c03500
J. Am. Chem. Soc. XXXX, XXX, XXX−XXX

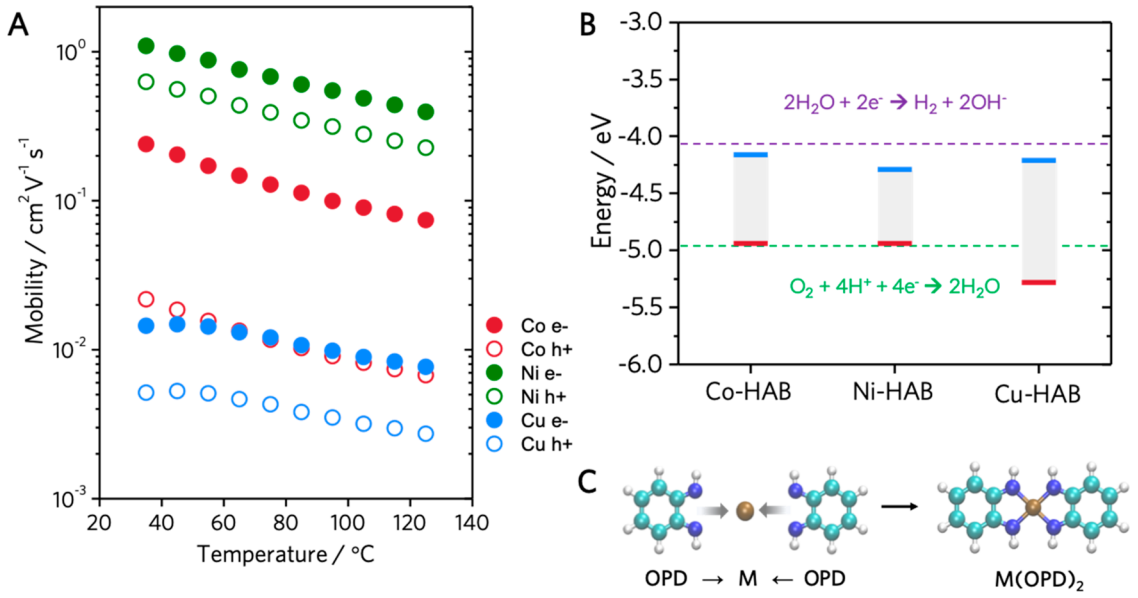

Figure 3. (A) Calculated mobilities of M-HABs under inert conditions. (B) HOMO (red) and LUMO (blue) levels of M-HAB MOFs relative to the vacuum level. Also shown are the redox potentials of O_2 (green) and H_2O (purple) at a pH of 7. (C) Schematic of the charge transfer simulation between the metal and ligand for the M-OPD (*o*-phenylenediamine) coordination model unit, M = Co, Ni, Cu.

$$\sigma_{E_0}(T) \propto \exp\left(-\frac{E_A}{k_B T}\right) \quad (2)$$

where E_A denotes the hopping energy. If the data conform to this model, $\log(\sigma_{E_0})$ should decrease linearly with inverse temperature. As shown in Figure 2B, all M-HABs exhibit excellent agreement with a hopping model under nitrogen conditions. The behavior of Co-HAB conforms to the hopping model under ambient conditions as well, with less than a 1 meV change to the activation energy. Cu-HAB and Ni-HAB exhibit ambient transport that is well-described by a hopping model at temperatures below 370 K (above 2.7 × $10^{-3}K^{-1}$), each with lower activation energies than those calculated for the transport under inert conditions. The drop in activation energy under ambient conditions is explained by the presence of physisorbed species, such as O_2 and H_2O, which can introduce midgap states, lowering the barrier for transport.[42] Above 370 K, the activation increases sharply for Cu-HAB as the physisorption becomes less stable. For Ni-HAB, the loss of physisorbed species results in a loss of carriers, and corresponding drop in conductivity above 370 K (below 2.7 × $10^{-3}K^{-1}$). The temperature dependent transport functions were used in conjunction with carrier effective masses estimated from the calculated band structures to determine approximate carrier mobilities in the MOFs, the results of which are depicted in Figure 3A (see Supporting Information for details). The key details of the band structure calculations are summarized in Table 1, and the band structures are depicted in the Supporting Information.

These mobilities explain the n-type behavior of all M-HAB MOFs under nitrogen conditions as exhibited in Figure 1C. Under inert conditions in an ideal MOF crystal, there should be equal numbers of n-type and p-type carriers as electrons at the valence band edge are thermally excited to the conduction band and generate holes. With carrier concentrations being equal, the Seebeck coefficient will reflect the carrier type with the highest mobility. As detailed in Table 1, larger bandwidths for electrons than those for holes in all cases result in a larger effective mass for holes in all M-HABs and thus a lower hole mobility than electron mobility, which explains the intrinsic n-type character of all M-HAB MOFs under inert conditions. As depicted in Figure 3A, only in Ni-HAB is the hole mobility high enough for hole transport to significantly contribute to overall conductivity which further corroborates its sole capability for ambipolar conduction.

Table 1. Calculated Band Structure Details for M-HAB MOFs

		Bandwidths (eV)		Effective Mass (m_e)	
MOF	Bandgap (eV)	Valence	Conduction	Holes	Electrons
Co-HAB	0.25	0.077	0.106	2.66	0.538
Ni-HAB	0.49	0.071	0.051	1.40	0.829
Cu-HAB	0.47	0.060	0.111	1.35	0.678

EXPERIMENTAL DETERMINATION OF ELECTRONIC STRUCTURE OF M-HABS

Photoemission spectroscopy in air (PESA) was performed to estimate the electronic structure of the MOFs in conjunction with the previously reported optical bandgaps for these materials.[14,36] The corresponding experimental energy levels of the MOFs are summarized in Figure 3B relative to the reduction potentials of oxygen and water. The discrepancy between the values reported in Figure 3B and Table 1 is attributed to the widening of the bandgap by limited particle size and defects and trap states associated with the experimental material relative to the idealized M-HAB structure used to calculate the data reported in Table 1.[37]

The air stability of organic materials is traditionally predicted by the position of the frontier orbitals relative to the redox potentials of O_2 and H_2O.[43] Oxygen and water will tend to pull away any electron density associated with occupied energy states above the reduction potentials of O_2 and H_2O. The highest occupied molecular orbital (HOMO) and the lowest unoccupied molecular orbital (LUMO) levels of all M-HABs lie below −4.02 eV, which suggests stability toward oxidation by water.[31,44] The air-stability of electronic operation of n-type organic semiconductors is principally governed by the position of the LUMO level.[44] The position of the LUMO

https://dx.doi.org/10.1021/jacs.0c03500
J. Am. Chem. Soc. XXXX, XXX, XXX−XXX

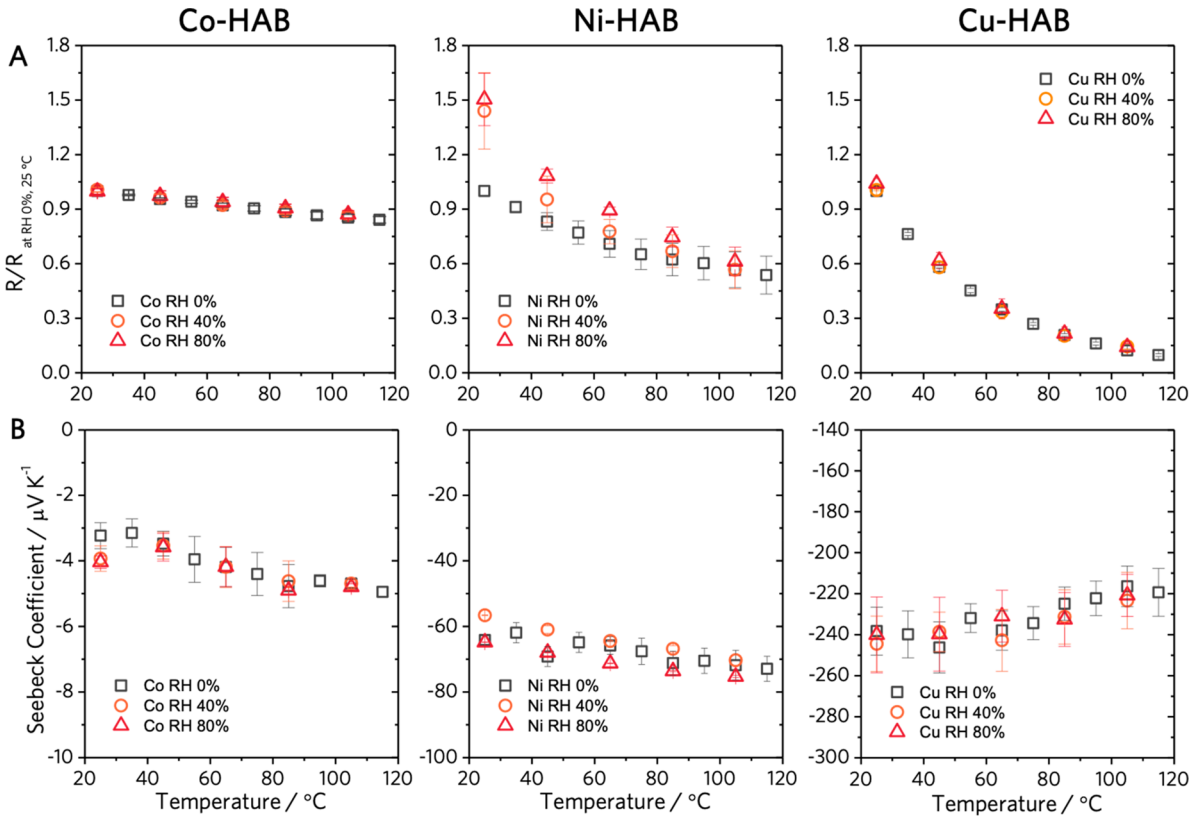

Figure 4. (A) Relative resistance and (B) Seebeck coefficient of M-HAB MOFs in an N_2/ H_2O environment with controlled humidity levels.

levels of all M-HABs well above the redox potential of O_2 predicts possible instability toward oxidation by atmospheric oxygen. The measurements suggest these materials can be either p- or n-type depending on the types of traps present.[45]

To isolate the effects of oxygen and water, the relative resistance and Seebeck coefficient of all M-HABs were measured in a controlled chamber under positive pressure of N_2 with a humidity monitor and a controlled flow rate of N_2-bubbled H_2O to achieve desired humidity levels. As shown in Figure 4B, the Seebeck coefficients of the M-HAB MOFs exhibit no dependence on humidity devoid of atmospheric oxygen. It can thus be inferred that oxygen is predominantly responsible for the change in Seebeck coefficient and conductivity for the M-HAB MOFs, in agreement with their frontier orbital positions relative to the redox potentials of O_2 and H_2O. The experimentally determined frontier orbital levels of MOFs relative to the redox potentials of O_2 and H_2O can thus be a possible metric to assess air stability of conductive MOFs.

According to previous accounts in the literature, the ligand in these M-HAB MOFs is the main site of redox activity.[36,46,47] Additionally, partial densities of states (PDOS) calculations (Figure S4) indicate that the conduction bands in all three M-HAB MOFs have zero complete states from the metal; thus the carriers in the conduction band are predominantly located on the ligand. Nevertheless, the choice of the metal atom dramatically impacts the conductance and air-stability of the resulting MOF. To understand this impact, we performed charge transfer analysis for coordination model units of both $M(HAB)_2$ and $M(OPD)_2$ (*o*-phenylenediamine) (Figure 3C). In the MOF structure, all amino groups are coordinated to metal ions. The electron density of a realistic coordination model unit is thus expected to lie somewhere between these two coordination model units. Table 2 lists the forward charge donation from ligand to metal ($\Delta Q_{[L\rightarrow M]}$), the charge transfer associated with back-bonding from metal to ligand ($\Delta Q_{[M\rightarrow L]}$), and the net charge transfer associated with formation of these coordination model units (ΔQ). The copper coordination model units feature the greatest forward donation of electron density of the three M-HABs studied, thereby depleting the

Table 2. Charge Transfer Analysis of M-HAB MOFs during Structure Formation

Structure	$\Delta Q_{[L\rightarrow M]}$ (e^-)	$\Delta Q_{[L\rightarrow M]}$ (e^-)	ΔQ (e^-)
$Cu(OPD)_2$	0.877	0.017	0.860
$Ni(OPD)_2$	0.0749	0.565	−0.450
$Co(OPD)_2$	0.197	0.0516	0.145
$Cu(HAB)_2$	2.09	0.810	1.28
$Ni(HAB)_2$	0.0935	0.100	−0.00685
$Co(HAB)_2$	0.178	0.167	0.0112

conduction band states on the ligand of mobile carriers, resulting in the lowest electrical conductivity of all M-HABs, as observed experimentally. With greater retentions of carriers at the ligand, Co-HAB and Ni-HAB achieve orders of magnitude higher conductivities than that of Cu-HAB. However, the electron density at the redox-active ligand is then available to react with O_2/H_2O under ambient conditions. Only the nickel coordination units have net back-bonding, which signifies that only in Ni-HAB do the majority of the mobile electrons sit on the ligand. Thus, only in Ni-HAB are the majority of the mobile electrons able to interact with O_2/H_2O, leaving a higher density of mobile holes than electrons under ambient conditions, causing the material to display p-type characteristics upon ambient exposure. The net forward donation for copper and cobalt model coordination units limits the electron density available at the ligand for interaction with adventitious species, thus these materials remain n-type under ambient conditions. However, the greater retention of n-type carriers on the HAB bound to Co relative to Cu results in a greater relative drop in conductivity when exposed to ambient conditions, as observed experimentally. Co-HAB retains less of its conductivity with ambient exposure than Ni-HAB because of its lower relative hole mobility.

These results can also be understood through a simplified *d*-orbital splitting model at the coordination sites. Determining the relative *d*-orbital energy levels in lower symmetry complexes like square planar

https://dx.doi.org/10.1021/jacs.0c03500
J. Am. Chem. Soc. XXXX, XXX, XXX−XXX

complexes is difficult due to the intricate parameters affecting *d*-orbital splitting; however, based on similar coordination complexes in the literature, we assume that the lowest and the highest *d*-orbitals are d_{xy} and $d_{x^2-y^2}$, respectively.[48] While this leaves many possible combinations for the remaining *d*-orbitals (d_{xz},d_{yz},d_{z^2}), these intermediate orbitals all have significant *z* character and will be henceforth referred to interchangeably as d_{iz}. Given that carrier transport in the MOF occurs primarily through delocalized orbitals parallel to but extending out in *z* from the lattice plane, the occupancy of the d_{iz} orbitals should greatly impact transport.[49,50] If the highest occupied *d*-orbital has significant *z* character, we would expect to see more significant carrier delocalization in the molecular orbitals (MO) associated with transport in the MOF and thus higher carrier mobility. The highest occupied *d*-orbitals in cobalt(II) and nickel(II) are d_{iz} orbitals.[48] The transport MO in Ni-HAB and Co-HAB should thus have some of the d_{iz} orbital character, resulting in extended transport orbitals parallel to the MOF sheet and relatively high mobility for carriers. Conversely, the highest occupied *d*-orbital in Cu-HAB is the $d_{x^2-y^2}$ orbital, leading to a less extended transport MO and lower inert mobility than those observed for Ni-HAB and Co-HAB, in agreement with the calculated results in Figure 3A.

The *d*-orbital argument can also predict the results of the charge transfer analysis and its implications for air-stability. The only partially unfilled orbital for copper(II) is an in-plane $d_{x^2-y^2}$, capable of σ-bonding interactions. When back-bonding occurs in a π-d coordination bond, the metal donates electron density to the antibonding orbitals on the ligand. The high effective nuclear charge on copper(II) stabilizes the out-of-plane d_{iz} orbitals and will prevent significant back-donation to the ligand, as shown in Table 2 for Cu-OPD. The more extensive π network of the model M-HAB unit relative to M-OPD lifts the energy levels of the d_{iz} orbitals and permits more back-donation as seen in the table for Cu-HAB. Nickel(II) has a fully unoccupied $d_{x^2-y^2}$ orbital, but the smaller effective nuclear charge on nickel(II) raises the energy of this orbital relative to copper(II), preventing significant forward σ-donation, as seen in Table 2.[48] Similarly, the fully occupied d_{iz} orbital on Ni(II) is destabilized relative to Cu(II), which should permit more extensive back-bonding to the ligand. Moreover, this back-bonding could generate vacancies in the out-of-plane orbitals on Ni(II) which would give rise to an extended network for both electron and hole transport. The intermediate nuclear charge on cobalt(II) should enable the fully unoccupied $d_{x^2-y^2}$ orbital to participate in σ-bonding, as well as forward donation to or back-donation from the half-occupied d_{iz} orbital.[48] Thus, more significant back-bonding occurs for Co-HAB than Co-OPD due to the raised energy levels of the d_{iz} orbitals from interaction with the more electron-rich HAB model unit.

CONCLUSION

In conclusion, we present a self-consistent model for metal cation-mediated carrier transport and air-stability in M-HABs: intrinsically conductive 2D MOF systems. Cu-HAB and Co-HAB represent the first MOFs to exhibit ambient n-type dominated transport, while Ni-HAB exhibits p-type transport in air and n-type transport under nitrogen conditions. The magnitude and air-dependence of the conductivity for the M-HAB system are theorized to vary with the energy and occupancy of the metal cation *d*-orbitals. On the basis of the experimental and calculated results, we propose that metal cations with significant *z* character in their frontier *d*-orbitals can increase the carrier delocalization in the orbitals associated with transport in the MOF and thereby increase the carrier mobility. Smaller effective nuclear charge on the metal cation enables more significant out-of-plane charge transfer, increasing the number of carriers for transport. However, charge transfer to the ligand undermines the air-stability of the MOF as O_2 reacts readily with the thermally excited electrons on the ligand that are otherwise available for conduction. We envision that the design perspectives discussed herein will enable new advances in MOF-based electronics.

ASSOCIATED CONTENT

Supporting Information

The Supporting Information is available free of charge at https://pubs.acs.org/doi/10.1021/jacs.0c03500.

Characterization details and additional experimental data (PDF)

AUTHOR INFORMATION

Corresponding Author

Zhenan Bao − *Department of Chemical Engineering, Stanford University, Stanford, California 94305, United States;* orcid.org/0000-0002-0972-1715; Email: zbao@stanford.edu

Authors

Allison C. Hinckley − *Department of Chemical Engineering, Stanford University, Stanford, California 94305, United States;* orcid.org/0000-0002-8829-3201

Jihye Park − *Department of Chemical Engineering, Stanford University, Stanford, California 94305, United States;* orcid.org/0000-0002-8644-2103

Joseph Gomes − *Department of Bioengineering, Stanford University, Stanford, California 94305, United States*

Evan Carlson − *Department of Chemical Engineering, Stanford University, Stanford, California 94305, United States*

Complete contact information is available at: https://pubs.acs.org/10.1021/jacs.0c03500

Author Contributions

#These authors contributed equally to this work.

Notes

The authors declare no competing financial interest.

ACKNOWLEDGMENTS

A.C.H. acknowledges support from the National Science Foundation Graduate Research Fellowship under Grant No. DGE-1147474. J.P. acknowledges support from the Dreyfus Foundation Postdoctoral Fellowship for Environmental Chemistry. Z.B. acknowledges support from US Department of Energy, Office Basic Energy Sciences, Division of Material Science and Engineering, Program on Physical Behaviors of Materials (DE-SC0016523). We thank Drs. Ze Zhang, Feifei Lian, and Prof. Eric Pop for fruitful discussion.

REFERENCES

(1) Campbell, M. G.; Sheberla, D.; Liu, S. F.; Swager, T. M.; Dincă, M. Cu3(Hexaiminotriphenylene)2: An Electrically Conductive 2D Metal-Organic Framework for Chemiresistive Sensing. *Angew. Chem., Int. Ed.* **2015**, *54* (14), 4349−4352.

(2) Clough, A. J.; Skelton, J. M.; Downes, C. A.; de la Rosa, A. A.; Yoo, J. W.; Walsh, A.; Melot, B. C.; Marinescu, S. C. Metallic Conductivity in a Two-Dimensional Cobalt Dithiolene Metal-Organic Framework. *J. Am. Chem. Soc.* **2017**, *139* (31), 10863−10867.

(3) Jia, H.; Yao, Y.; Zhao, J.; Gao, Y.; Luo, Z.; Du, P. A Novel Two-Dimensional Nickel Phthalocyanine-Based Metal-Organic Framework for Highly Efficient Water Oxidation Catalysis. *J. Mater. Chem. A* **2018**, *6* (3), 1188−1195.

(4) Kambe, T.; Sakamoto, R.; Hoshiko, K.; Takada, K.; Miyachi, M.; Ryu, J.-H.; Sasaki, S.; Kim, J.; Nakazato, K.; Takata, M.; Nishihara, H.

π-Conjugated Nickel Bis(Dithiolene) Complex Nanosheet. *J. Am. Chem. Soc.* **2013**, *135* (7), 2462−2465.
(5) Kobayashi, Y.; Jacobs, B.; Allendorf, M. D.; Long, J. R. Conductivity, Doping, and Redox Chemistry of a Microporous Dithiolene-Based Metal-Organic Framework. *Chem. Mater.* **2010**, *22* (14), 4120−4122.
(6) Lahiri, N.; Lotfizadeh, N.; Tsuchikawa, R.; Deshpande, V. V.; Louie, J. Hexaaminobenzene as a Building Block for a Family of 2D Coordination Polymers. *J. Am. Chem. Soc.* **2017**, *139* (1), 19−22.
(7) Sheberla, D.; Sun, L.; Blood-Forsythe, M. A.; Er, S.; Wade, C. R.; Brozek, C. K.; Aspuru-Guzik, A.; Dincă, M. High Electrical Conductivity in Ni3(2,3,6,7,10,11-Hexaiminotriphenylene)2, a Semiconducting Metal-Organic Graphene Analogue. *J. Am. Chem. Soc.* **2014**, *136* (25), 8859−8862.
(8) Sheberla, D.; Bachman, J. C.; Elias, J. S.; Sun, C.-J.; Shao-Horn, Y.; Dinca, M. Conductive MOF Electrodes for Stable Supercapacitors with High Areal Capacitance. *Nat. Mater.* **2017**, *16* (2), 220−224.
(9) Xing, H.; Shuai, Z.; Liyao, L.; Lei, Y.; Genfu, C.; Wei, X.; Daoben, Z. Superconductivity in a Copper(II)-Based Coordination Polymer with Perfect Kagome Structure. *Angew. Chem., Int. Ed.* **2018**, *57* (1), 146−150.
(10) Darago, L. E.; Aubrey, M. L.; Yu, C. J.; Gonzalez, M. I.; Long, J. R. Electronic Conductivity, Ferrimagnetic Ordering, and Reductive Insertion Mediated by Organic Mixed-Valence in a Ferric Semiquinoid Metal-Organic Framework. *J. Am. Chem. Soc.* **2015**, *137* (50), 15703−15711.
(11) DeGayner, J. A.; Jeon, I.-R.; Sun, L.; Dincă, M.; Harris, T. D. 2D Conductive Iron-Quinoid Magnets Ordering up to Tc = 105 K via Heterogenous Redox Chemistry. *J. Am. Chem. Soc.* **2017**, *139* (11), 4175−4184.
(12) Dong, R.; Pfeffermann, M.; Liang, H.; Zheng, Z.; Zhu, X.; Zhang, J.; Feng, X. Large-Area, Free-Standing, Two-Dimensional Supramolecular Polymer Single-Layer Sheets for Highly Efficient Electrocatalytic Hydrogen Evolution. *Angew. Chem., Int. Ed.* **2015**, *54* (41), 12058−12063.
(13) Dou, J.; Sun, L.; Ge, Y.; Li, W.; Hendon, C. H.; Li, J.; Gul, S.; Yano, J.; Stach, E. A.; Dincă, M. Signature of Metallic Behavior in the Metal-Organic Frameworks M 3 (Hexaiminobenzene) 2 (M = Ni, Cu). *J. Am. Chem. Soc.* **2017**, *139* (39), 13608−13611.
(14) Feng, D.; Lei, T.; Lukatskaya, M. R.; Park, J.; Huang, Z.; Lee, M.; Shaw, L.; Chen, S.; Yakovenko, A. A.; Kulkarni, A.; Xiao, J.; Fredrickson, K.; Tok, J. B.; Zou, X.; Cui, Y.; Bao, Z. Robust and Conductive Two-Dimensional Metal-organic Frameworks with Exceptionally High Volumetric and Areal Capacitance. *Nat. Energy* **2018**, *3* (1), 30−36.
(15) Hisanori, N.; Nobuhiro, Y.; Teppei, Y.; Kanji, S.; Nobuo, K. Synthesis and Electric Properties of a Two-Dimensional Metal-Organic Framework Based on Phthalocyanine. *Chem. - Eur. J.* **2018**, *24* (8), 1806−1810.
(16) Hmadeh, M.; Lu, Z.; Liu, Z.; Gándara, F.; Furukawa, H.; Wan, S.; Augustyn, V.; Chang, R.; Liao, L.; Zhou, F.; Perre, E.; Vidvuds, O.; Suenaga, K.; Duan, X.; Dunn, B.; Yamamto, Y.; Terasaki, O.; Yaghi, O. M. New Porous Crystals of Extended Metal-Catecholates. *Chem. Mater.* **2012**, *24* (18), 3511−3513.
(17) Huang, X.; Sheng, P.; Tu, Z.; Zhang, F.; Wang, J.; Geng, H.; Zou, Y.; Di, C.; Yi, Y.; Sun, Y.; Xu, W.; Zhu, D. A Two-Dimensional π-d Conjugated Coordination Polymer with Extremely High Electrical Conductivity and Ambipolar Transport Behaviour. *Nat. Commun.* **2015**, *6*, 7408 .
(18) Xie, L. S.; Skorupskii, G.; Dincă, M. Electrically Conductive Metal-Organic Frameworks. *Chemical Reviews*. American Chemical Society 2020, DOI: 10.1021/acs.chemrev.9b00766.
(19) Li, W.-H.; Deng, W.-H.; Wang, G.-E.; Xu, G. Conductive MOFs. *EnergyChem.* **2020**, *2* (2), 100029.
(20) Deng, X.; Hu, J. Y.; Luo, J.; Liao, W. M.; He, J. Conductive Metal-Organic Frameworks: Mechanisms, Design Strategies and Recent Advances. *Top. Curr. Chem.* 2020, *378*, 1−50, DOI: 10.1007/s41061-020-0289.
(21) Liang, Z.; Zhao, R.; Qiu, T.; Zou, R.; Xu, Q. Metal-Organic Framework-Derived Materials for Electrochemical Energy Applications. *EnergyChem.* **2019**, *1* (1), 100001.
(22) Xiao, X.; Zou, L.; Pang, H.; Xu, Q. Synthesis of Micro/Nanoscaled Metal-Organic Frameworks and Their Direct Electrochemical Applications. *Chem. Soc. Rev.* 2020, *49*,301−331, DOI: 10.1039/c7cs00614d.
(23) Li, X.; Yang, X.; Xue, H.; Pang, H.; Xu, Q. Metal-Organic Frameworks as a Platform for Clean Energy Applications. *EnergyChem.* **2020**, *2* (2), 100027.
(24) Xu, Y.; Li, Q.; Xue, H.; Pang, H. Metal-Organic Frameworks for Direct Electrochemical Applications. *Coord. Chem. Rev.* 2018, *376*, 292−318, DOI: 10.1016/j.ccr.2018.08.010.
(25) Wang, J.; Li, N.; Xu, Y.; Pang, H. Two-Dimensional MOF and COF Nanosheets: Synthesis and Applications in Electrochemistry. *Chem. - Eur. J.* **2020**, *26* (29), 6402−6422.
(26) Stassen, I.; Burtch, N.; Talin, A.; Falcaro, P.; Allendorf, M.; Ameloot, R. An Updated Roadmap for the Integration of Metal-Organic Frameworks with Electronic Devices and Chemical Sensors. *Chem. Soc. Rev.* **2017**, *46* (11), 3185−3241.
(27) Wang, X.; Zhang, X.; Sun, L.; Lee, D.; Lee, S.; Wang, M.; Zhao, J.; Shao-Horn, Y.; Dincă, M.; Palacios, T.; Gleason, K. K. High Electrical Conductivity and Carrier Mobility in OCVD PEDOT Thin Films by Engineered Crystallization and Acid Treatment. *Sci. Adv.* **2018**, *4* (9), No. eaat5780.
(28) Pathak, A.; Shen, J.-W.; Usman, M.; Wei, L.-F.; Mendiratta, S.; Chang, Y.-S.; Sainbileg, B.; Ngue, C.-M.; Chen, R.-S.; Hayashi, M.; Luo, T.-T.; Chen, F.-R.; Chen, K.-H.; Tseng, T.-W.; Chen, L.-C; Lu, K.-L. Integration of a (-Cu-S-)n Plane in a Metal-Organic Framework Affords High Electrical Conductivity. *Nat. Commun.* **2019**, *10* (1), 1721.
(29) Burroughes, J. H.; Bradley, D. D. C.; Brown, A. R.; Marks, R. N.; Mackay, K.; Friend, R. H.; Burns, P. L.; Holmes, A. B. Light-Emitting Diodes Based on Conjugated Polymers. *Nature* **1990**, *347* (6293), 539−541.
(30) Marks, T. J. Materials for Organic and Hybrid Inorganic/Organic Electronics. *MRS Bull.* **2010**, *35* (12), 1018−1027.
(31) de Leeuw, D. M.; Simenon, M. M. J.; Brown, A. R.; Einerhand, R. E. F. Stability of N-Type Doped Conducting Polymers and Consequences for Polymeric Microelectronic Devices. *Synth. Met.* **1997**, *87* (1), 53−59.
(32) Russ, B.; Glaudell, A.; Urban, J. J.; Chabinyc, M. L.; Segalman, R. A. Organic Thermoelectric Materials for Energy Harvesting and Temperature Control. *Nat. Rev. Mater.* **2016**, *1*, 16050.
(33) Bao, Z.; Lovinger, A. J.; Brown, J. New Air-Stable *n* -Channel Organic Thin Film Transistors. *J. Am. Chem. Soc.* **1998**, *120* (1), 207−208.
(34) Park, S. S.; Hontz, E. R.; Sun, L.; Hendon, C. H.; Walsh, A.; Van Voorhis, T.; Dincă, M. Cation-Dependent Intrinsic Electrical Conductivity in Isostructural Tetrathiafulvalene-Based Microporous Metal-Organic Frameworks. *J. Am. Chem. Soc.* **2015**, *137* (5), 1774−1777.
(35) He, Y.; Spataru, C. D.; Léonard, F.; Jones, R. E.; Foster, M. E.; Allendorf, M. D.; Alec Talin, A. Two-Dimensional Metal-Organic Frameworks with High Thermoelectric Efficiency through Metal Ion Selection. *Phys. Chem. Chem. Phys.* **2017**, *19* (29), 19461−19467.
(36) Park, J.; Lee, M.; Feng, D.; Huang, Z.; Hinckley, A. C.; Yakovenko, A.; Zou, X.; Cui, Y.; Bao, Z. Stabilization of Hexaaminobenzene in a 2D Conductive Metal-Organic Framework for High Power Sodium Storage. *J. Am. Chem. Soc.* **2018**, *140* (32), 10315−10323.
(37) Sun, L.; Liao, B.; Sheberla, D.; Kraemer, D.; Zhou, J.; Stach, E. A.; Zakharov, D.; Stavila, V.; Talin, A. A.; Ge, Y.; Allendorf, M. D.; Chen, G.; Léonard, F.; Dincă, M. A Microporous and Naturally Nanostructured Thermoelectric Metal-Organic Framework with Ultralow Thermal Conductivity. *Joule* **2017**, *1* (1), 168−177.
(38) Erickson, K. J.; Léonard, F.; Stavila, V.; Foster, M. E.; Spataru, C. D.; Jones, R. E.; Foley, B. M.; Hopkins, P. E.; Allendorf, M. D.; Talin, A. A. Thin Film Thermoelectric Metal-Organic Framework

https://dx.doi.org/10.1021/jacs.0c03500
J. Am. Chem. Soc. XXXX, XXX, XXX−XXX

with High Seebeck Coefficient and Low Thermal Conductivity. *Adv. Mater.* **2015**, *27* (22), 3453−3459.
(39) Anthopoulos, T. D.; Anyfantis, G. C.; Papavassiliou, G. C.; de Leeuw, D. M. Air-Stable Ambipolar Organic Transistors. *Appl. Phys. Lett.* **2007**, *90* (12), 122105.
(40) Wu, G.; Huang, J.; Zang, Y.; He, J.; Xu, G. Porous Field-Effect Transistors Based on a Semiconductive Metal-Organic Framework. *J. Am. Chem. Soc.* **2017**, *139* (4), 1360−1363.
(41) Kang, S. D.; Snyder, G. J. Charge-Transport Model for Conducting Polymers. *Nat. Mater.* **2017**, *16* (2), 252−257.
(42) Stallinga, P. *Electrical Characterization of Organic Electronic Materials and Devices*; Wiley, 2009.
(43) Shan, B.; Miao, Q. Molecular Design of N-Type Organic Semiconductors for High-Performance Thin Film Transistors. *Tetrahedron Lett.* **2017**, *58* (20), 1903−1911.
(44) Usta, H.; Risko, C.; Wang, Z.; Huang, H.; Deliomeroglu, M. K.; Zhukhovitskiy, A.; Facchetti, A.; Marks, T. J. Design, Synthesis, and Characterization of Ladder-Type Molecules and Polymers. Air-Stable, Solution-Processable *n* -Channel and Ambipolar Semiconductors for Thin-Film Transistors via Experiment and Theory. *J. Am. Chem. Soc.* **2009**, *131* (15), 5586−5608.
(45) Tang, M. L.; Reichardt, A. D.; Wei, P.; Bao, Z. Correlating Carrier Type with Frontier Molecular Orbital Energy Levels in Organic Thin Film Transistors of Functionalized Acene Derivatives. *J. Am. Chem. Soc.* **2009**, *131* (14), 5264−5273.
(46) Herebian, D.; Bothe, E.; Neese, F.; Weyhermuller, T.; Wieghardt, K. Molecular and Electronic Structures of Bis-(o-Diiminobenzosemiquinonato)Metal(II) Complexes (Ni, Pd, Pt), Their Monocations and -Anions, and of Dimeric Dications Containing Weak Metal-Metal Bonds. *J. Am. Chem. Soc.* **2003**. *125*9116.
(47) Miner, E. M.; Gul, S.; Ricke, N. D.; Pastor, E.; Yano, J.; Yachandra, V. K.; Van Voorhis, T.; Dincă, M. Mechanistic Evidence for Ligand-Centered Electrocatalytic Oxygen Reduction with the Conductive MOF Ni_3 (Hexaiminotriphenylene) $_2$. *ACS Catal.* **2017**, *7* (11), 7726−7731.
(48) Nishida, Y.; Kida, S. Splitting of D-Orbitals in Square Planar Complexes of Copper(II), Nickel(II) and Cobalt(II). *Coord. Chem. Rev.* **1979**, *27* (3), 275−298.
(49) Hendon, C. H.; Tiana, D.; Walsh, A. Conductive Metal-Organic Frameworks and Networks: Fact or Fantasy? *Phys. Chem. Chem. Phys.* **2012**, *14* (38), 13120−13132.
(50) Dou, J. H.; Sun, L.; Ge, Y.; Li, W.; Hendon, C. H.; Li, J.; Gul, S.; Yano, J.; Stach, E. A.; Dincă, M. Signature of Metallic Behavior in the Metal-Organic Frameworks M3(Hexaiminobenzene)2 (M = Ni, Cu). *J. Am. Chem. Soc.* **2017**, *139* (39), 13608−13611.

https://dx.doi.org/10.1021/jacs.0c03500
J. Am. Chem. Soc. XXXX, XXX, XXX−XXX